Research Article | Vol. 8, No. 7 | 1 Jul 2017 | BIOMEDICAL OPTICS EXPRESS 3232
Biomedical Optics EXPRESS

Electrically tunable fluidic lens imaging system for laparoscopic fluorescence-guided surgery

DAVIDE VOLPI,* IAIN D. C. TULLIS, PAUL R. BARBER, EDYTA M. AUGUSTYNIAK, SEAN C. SMART, KATHERINE A. VALLIS, AND BORIVOJ VOJNOVIC

CR-UK/MRC Oxford Institute for Radiation Oncology, Department of Oncology, University of Oxford, Oxford, OX3 7DQ, UK
**davide.volpi@oncology.ox.ac.uk*

Abstract: The addition of fluorescence guidance in laparoscopic procedures has gained significant interest in recent years, particularly through the use of near infrared (NIR) markers. In this work we present a novel laparoscope camera coupler based on an electrically tunable fluidic lens that permits programmable focus control and has desirable achromatic performance from the visible to the NIR. Its use extends the lower working distance limit and improves detection sensitivity, important for work with molecularly targeted fluorescence markers. We demonstrate its superior optical performance in laparoscopic fluorescence-guided surgery. *In vivo* results using a tumor specific molecular probe and a nonspecific NIR dye are presented.

OCIS codes: (170.0110) Imaging systems; (170.2150) Endoscopic imaging; (170.6280) Spectroscopy, fluorescence and luminescence; (120.3620) Lens system design; (120.4820) Optical systems.

References and links

1. U. Berggren, T. Gordh, D. Grama, U. Haglund, J. Rastad, and D. Arvidsson, "Laparoscopicversus open cholecystectomy: Hospitalization, sick leave, analgesia and trauma responses," Br. J. Surg. **81**(9), 1362–1365 (1994).
2. C. P. Delaney, E. Chang, A. J. Senagore, and M. Broder, "Clinical outcomes and resource utilization associated with laparoscopic and open colectomy using a large national database," Ann. Surg. **247**(5), 819–824 (2008).
3. V. Mais, S. Ajossa, S. Guerriero, M. Mascia, E. Solla, and G. B. Melis, "Laparoscopic versus abdominal myomectomy: a prospective, randomized trial to evaluate benefits in early outcome," Am. J. Obstet. Gynecol. **174**(2), 654–658 (1996).
4. J. Rassweiler, O. Seemann, M. Schulze, D. Teber, M. Hatzinger, and T. Frede, "Laparoscopic versus open radical prostatectomy: A comparative study at a single institution," J. Urol. **169**(5), 1689–1693 (2003).
5. A. C. Schlaerth and N. R. Abu-Rustum, "Role of minimally invasive surgery in gynecologic cancers," Oncologist **11**(8), 895–901 (2006).
6. A. L. Vahrmeijer, M. Hutteman, J. R. van der Vorst, C. J. H. van de Velde, and J. V. Frangioni, "Image-guided cancer surgery using near-infrared fluorescence," Nat. Rev. Clin. Oncol. **10**(9), 507–518 (2013).
7. A. Laios, D. Volpi, I. D. Tullis, M. Woodward, S. Kennedy, P. N. Pathiraja, K. Haldar, B. Vojnovic, and A. A. Ahmed, "A prospective pilot study of detection of sentinel lymph nodes in gynaecological cancers using a novel near infrared fluorescence imaging system," BMC Res. Notes **8**(1), 608 (2015).
8. J. V. Frangioni, "In vivo near-infrared fluorescence imaging," Curr. Opin. Chem. Biol. **7**(5), 626–634 (2003).
9. J. Glatz, J. Varga, P. B. Garcia-Allende, M. Koch, F. R. Greten, and V. Ntziachristos, "Concurrent video-rate color and near-infrared fluorescence laparoscopy," J. Biomed. Opt. **18**(10), 101302 (2013).
10. B. Vojnovic, "An electrically-tuneable achromatic laparoscope imaging lens" (2017), retrieved http://users.ox.ac.uk/~atdgroup/technicalnotes/An%20electrically-tuneable%20achromatic%20laparoscope%20imaging%20lens.pdf.
11. E. L. Jewell, J. J. Huang, N. R. Abu-Rustum, G. J. Gardner, C. L. Brown, Y. Sonoda, R. R. Barakat, D. A. Levine, and M. M. Leitao, Jr., "Detection of sentinel lymph nodes in minimally invasive surgery using indocyanine green and near-infrared fluorescence imaging for uterine and cervical malignancies," Gynecol. Oncol. **133**(2), 274–277 (2014).
12. G. H. KleinJan, N. S. van den Berg, O. R. Brouwer, J. de Jong, C. Acar, E. M. Wit, E. Vegt, V. van der Noort, R. A. Valdés Olmos, F. W. van Leeuwen, and H. G. van der Poel, "Optimisation of Fluorescence Guidance During Robot-assisted Laparoscopic Sentinel Node Biopsy for Prostate Cancer," Eur. Urol. **66**(6), 991–998 (2014).

#291841 https://doi.org/10.1364/BOE.8.003232
Journal © 2017 Received 31 Mar 2017; revised 24 May 2017; accepted 24 May 2017; published 13 Jun 2017

Biomedical Optics EXPRESS

13. T. Ishizawa, Y. Bandai, M. Ijichi, J. Kaneko, K. Hasegawa, and N. Kokudo, "Fluorescent cholangiography illuminating the biliary tree during laparoscopic cholecystectomy," Br. J. Surg. **97**(9), 1369–1377 (2010).
14. T. M. Yeung, D. Volpi, I. D. C. Tullis, G. A. Nicholson, N. Buchs, C. Cunningham, R. Guy, I. Lindsey, B. George, O. Jones, L. Mun Wang, R. Hompes, B. Vojnovic, F. Hamdy, and N. J. Mortensen, "Identifying Ureters In Situ Under Fluorescence During Laparoscopic and Open Colorectal Surgery," Ann. Surg. **263**(1), e1–e2 (2016).
15. O. J. Wagner, B. E. Louie, E. Vallières, R. W. Aye, and A. S. Farivar, "Near-Infrared Fluorescence Imaging Can Help Identify the Contralateral Phrenic Nerve During Robotic Thymectomy," Ann. Thorac. Surg. **94**(2), 622–625 (2012).
16. M. Garland, J. J. Yim, and M. Bogyo, "A Bright Future for Precision Medicine: Advances in Fluorescent Chemical Probe Design and Their Clinical Application," Cell Chem Biol **23**(1), 122–136 (2016).
17. S. Friberg and S. Mattson, "On the growth rates of human malignant tumors: implications for medical decision making," J. Surg. Oncol. **65**(4), 284–297 (1997).
18. H. S. Tran Cao, S. Kaushal, C. Lee, C. S. Snyder, K. J. Thompson, S. Horgan, M. A. Talamini, R. M. Hoffman, and M. Bouvet, "Fluorescence laparoscopy imaging of pancreatic tumor progression in an orthotopic mouse model," Surg. Endosc. **25**(1), 48–54 (2011).
19. D. C. Gray, E. M. Kim, V. E. Cotero, A. Bajaj, V. P. Staudinger, C. A. T. Hehir, and S. Yazdanfar, "Dual-mode laparoscopic fluorescence image-guided surgery using a single camera," Biomed. Opt. Express **3**(8), 1880–1890 (2012).
20. V. Venugopal, M. Park, Y. Ashitate, F. Neacsu, F. Kettenring, J. V. Frangioni, S. P. Gangadharan, and S. Gioux, "Design and characterization of an optimized simultaneous color and near-infrared fluorescence rigid endoscopic imaging system," J. Biomed. Opt. **18**(12), 126018 (2013).
21. D. Volpi, I. D. C. Tullis, A. Laios, P. N. J. Pathiraja, K. Haldar, A. A. Ahmed, and B. Vojnovic, "A novel multiwavelength fluorescence image-guided surgery imaging system," Proc. SPIE Advanced Biomedical and Clinical Diagnostic Systems XII **8935**, (2014).
22. J. C. Tesar, P. Cottle, and J. P. Fengler, "Compensating optical coupler for visible and nir imaging," U.S. Patent US20110249323 (2011).
23. Q. Wang, A. Khanicheh, D. Leiner, D. Shafer, and J. Zobel, "Endoscope field of view measurement," Biomed. Opt. Express **8**(3), 1441–1454 (2017).
24. J. Glatz, P. Symvoulidis, P. Beatriz Garcia-Allende, and V. Ntziachristos, "Robust overlay schemes for the fusion of fluorescence and color channels in biological imaging," J. Biomed. Opt. **19**(4), 040501 (2014).
25. E. H. K. Stelzer, "Contrast, resolution, pixelation, dynamic range and signal-to-noise ratio: fundamental limits to resolution in fluorescence light microscopy," J Microsc-Oxford **189**(1), 15–24 (1998).
26. M. R. Anderson, R. Harrison, P. A. Atherfold, M. J. Campbell, S. J. Darnton, J. Obszynska, and J. A. Z. Jankowski, "Met receptor signaling: a key effector in esophageal adenocarcinoma," Clin. Cancer Res. **12**(20), 5936–5943 (2006).
27. S. Liu, Y. Zheng, D. Volpi, M. El-Kasti, D. Klotz, I. Tullis, A. Henricks, L. Campo, K. Myers, A. Laios, P. Thomas, T. Ng, S. Dhar, C. Becker, B. Vojnovic, and A. A. Ahmed, "Toward Operative In Vivo Fluorescence Imaging of the c-Met Proto-Oncogene for Personalization of Therapy in Ovarian Cancer," Cancer **121**(2), 202–213 (2015).
28. J. P. Fengler and P. Westwick, B. A.E., and C. P., "Imaging system for combined full-color reflectance and near-infrared imaging," U.S. Patent US20110063427 (2009).
29. Y. Qin and H. Hua, "Continuously zoom imaging probe for the multi-resolution foveated laparoscope," Biomed. Opt. Express **7**(4), 1175–1182 (2016).
30. F. S. Tsai, D. Johnson, C. S. Francis, S. H. Cho, W. Qiao, A. Arianpour, Y. Mintz, S. Horgan, M. Talamini, and Y. H. Lo, "Fluidic lens laparoscopic zoom camera for minimally invasive surgery," J. Biomed. Opt. **15**(3), 030504 (2010).
31. S. Lee, M. Choi, E. Lee, K. D. Jung, J. H. Chang, and W. Kim, "Four zoom lens design for 3D laparoscope by using liquid lens," Zoom Lenses Iv **8488**(2012).
32. A. Nishikawa, H. Nakagoe, K. Taniguchi, Y. Yamada, M. Sekimoto, S. Takiguchi, M. Monden, and F. Miyazaki, "How Does the Camera Assistant Decide the Zooming Ratio of Laparoscopic Images? Analysis and Implementation," in *Medical Image Computing and Computer-Assisted Intervention – MICCAI 2008: 11th International Conference, New York, NY, USA, September 6–10, 2008, Proceedings, Part II*, D. Metaxas, L. Axel, G. Fichtinger, and G. Székely, eds. (Springer Berlin Heidelberg, Berlin, Heidelberg, 2008), pp. 611–618.

1. Introduction

Minimally invasive surgery (MIS) has been shown to be safe and effective in a wide range of surgical procedures, while providing considerable benefits for the patient including smaller incisions, reduced pain and shorter hospital stays [1–5]. Conventional laparoscopes provide visual access to the surgical field by illuminating the region of interest with white light and imaging the scene back through a relay lens imaging channel, allowing standard color cameras to acquire images for display in real time. The relay lenses are commonly constructed according to the Hopkins 'thick lens' principle and are complemented by an

Biomedical Optics EXPRESS

objective lens and an eyepiece. The eyepiece 'output' is focused using an imaging lens onto one or more imaging chips which are used to collect information to display on one or more monitors. White light color reflectance imaging allows the surgeon to visually differentiate between healthy and diseased tissue. In the case of small or low contrast lesions, correct identification of the disease can be challenging. For this reason, additional methods to improve contrast are becoming more popular; these also place extra demands on the optical imaging system.

The use of fluorescence as an additional contrast mechanism during surgery is gaining increasing interest from the medical community, particularly in oncology [6]. Fluorescence can enhance the view of the surgical field by providing cellular and molecular information as well as structural and perfusion-related information. In addition, the technology can be readily fitted to existing laparoscopic instrumentation, with minimal interference with standard surgical procedures. As with reflected white light, fluorescence imaging in the visible can only investigate the tissue surface due to the poor penetration depth of visible light and its contrast is restricted by tissue autofluorescence. The former is a secondary issue in surgery, where intrinsic access to the imaging field is usually provided as the surgery progresses.

The use of fluorescence in the near infrared (NIR) spectral region has shown that penetration depths of the order of 10s of mm can be achieved [7], at the expense of poorer spatial resolution. More importantly, autofluorescence is significantly reduced [8]. Although light from deeper targets is inevitably scattered, suggesting that imaging at these long wavelengths need not be parfocal with visible light imaging, superficial targets are considerably brighter and here achromatic performance of the optics is necessary. Transmission in conventional MIS systems is, however, generally optimized for the visible part of the spectrum only [9], although laparoscopes with good transmission in the NIR are becoming available [10].

Fluorescence-guided surgery (FGS) in the NIR has been successfully performed in a number of laparoscopic procedures including sentinel lymph node (SLN) detection [7, 11, 12], cholangiography [13], ureter imaging [14] and nerve identification [15] amongst others. These advances have been driven by the availability of fluorescent dyes that are approved for clinical use in off-label studies (i.e. indocyanine green (ICG) and methylene blue (MB)) and by the emergence of suitable imaging systems and associated excitation devices. Recent efforts towards development of NIR fluorophores and tumor biomarkers have shown a clear push towards the use of fluorescence molecular imaging (FMI) during cancer surgery [16]. Here, sensitivity is crucial and usually achieved by decreasing working distances and thus increasing light collection. Molecular agents can specifically target tumor or healthy tissue and therefore allow fluorescence detection of structures that are typically not visible under reflected light. FMI has the potential to achieve the detection of a tumor before it reaches a size corresponding to the diagnostic level of conventional imaging modalities (~10^7 – 10^9 cells, 0.01 – 1 cm^3) [17].

A number of in-house developed laparoscopic systems for FGS have been described by various research groups [9, 18–21]. The aim of such systems is to overcome the sensitivity and spectral limitations of commercial counterparts, which tend to focus on usability and ergonomics. Such systems face the challenge of translating their technologies into a clinical environment, where ergonomics and simplicity of use become increasingly important.

In this work, we present a novel optical imaging accessory designed to be used with in-house developed laparoscopic FGS devices and optimized for operating in the visible and NIR spectral regions. Our system addresses two problems. Firstly, in a surgical environment, surgeons are reluctant to adjust the coupler focus as most cameras/couplers are placed within a sterile sheath. Furthermore, development of mechanically-activated focusing systems is not a trivial task faced by researchers when implementing novel imaging approaches capable of operating reliably in a surgical environment. Such refocusing is, however, necessary when working distances are reduced as is the case for FMI. Secondly, achromatic performance,

Biomedical Optics EXPRESS

desirable to aid navigation and to maximize NIR fluorescence detection, is rarely addressed in published work, though commercial developments have been described, albeit using complex prism arrangements [22], not readily able to be duplicated by other researchers.

We present means towards addressing these problems by describing an electrically tunable achromatic lens system. The ability to control lens focus is a prerequisite for an autofocus system, aimed at the first problem. Furthermore, our approach requires simple electrical 'up-down' switches to control system focus, rather than complex mechanics. Secondly, the achromaticity of our tunable lens system (TLS) already improves the combined performance when coupled to a laparoscope. Moreover, it paves the way for further correcting the chromatic shift associated with the laparoscope itself. This has been achieved by using off-the-shelf optical components throughout, ensuring that this system can be replicated by others. The capability of the system is demonstrated *in vivo* and comparison is made with a previously developed device aimed at white reflectance and multi-spectral fluorescence detection [21].

2. Methods

2.1 Laparoscope characterization

The rigid endoscope used in this work is a 10 mm diameter, 300 mm long, zero degrees viewing angle, Hopkins rod lens-based laparoscope optimized for NIR use (26003AGA, Karl Storz, Tuttlingen, Germany). Wideband optical coatings on its internal components extend operation well into the NIR [10]. It includes the possibility of switching in a 472 nm long-pass or a 660 – 825 nm FWHM excitation blocking filters and allows operation without any internal filters switched in. In this work neither of these filters were used. The laparoscope exit pupil and output ray fan were determined, as shown in Fig. 1, to allow the design of the TLS. Output pupil diameter was measured by placing the laparoscope tip ~200 mm away from two point sources located at the edges of the field of view at diagonally opposed positions. Each source produced a hemi-isotropic beam and, resulting in near-collimated beams at the eyepiece. A 1/3" CCD camera (BFLY-U3-13S2M-CS, Point Grey, Richmond, Canada) with a 25 mm focal length imaging lens (#67-715, Edmund Optics, Barrington, NJ, USA) was placed 200 mm from an opaque observation screen and focused to image the screen. The camera and screen arrangement was coaxial with the eyepiece. The laparoscope formed two circular images on the screen corresponding to the two point sources. The screen was moved along the optical axis relative to the eyepiece until the two images overlapped, thus providing the exit pupil location. The exit pupil diameter and position on the optical axis were respectively 2.8 mm ± 0.1 mm and 1.75 mm ± 0.1 mm away from the eyepiece flat surface. The maximum eyepiece field angle was ± 7 degrees ± 0.1 degrees. Changes of these values of up to ± 0.2 mm and ± 0.3 degree did not materially change the performance of the model described in §2.2.2.

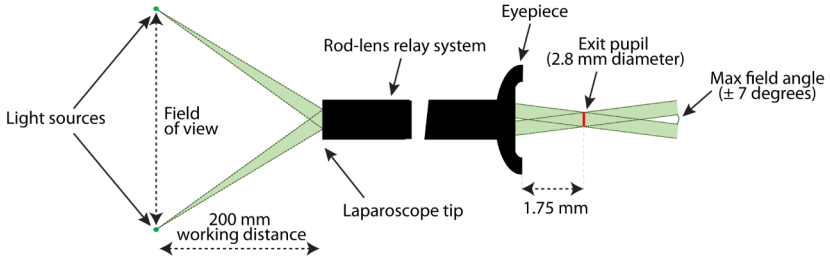

Fig. 1. Schematic representation showing the properties of the laparoscope exit pupil. Note that the drawing is not to scale for the sake of clarity.

Biomedical Optics EXPRESS

2.2 Laparoscopic tunable lens system (TLS)

2.2.1 Focus-tunable element

The laparoscopic tunable lens system (TLS) described in this work is based on a 10 mm clear aperture, 30 mm diameter electrically focus-tunable fluidic lens (EL-10-30-TC (beta version), Optotune, Dietikon, Switzerland). This lens was chosen due to its large optical aperture, as required by the laparoscope exit pupil beam divergence. In addition, this lens provides a convenient range of focal lengths (~65-180 mm) and incorporates a temperature sensor for compensation of slight focal length variations due to thermal effects. The lens focal length was electrically controlled such that, once set to the user-required value, it is maintained at that value. For this purpose, we developed a microcontroller-based driver that extracted, via an I^2C bus (http://i2c.info/i2c-bus-specification), the manufacturer's calibration table of current to diopter settings over a range of temperatures and computed drive current for a given focal length. This drive was provided by an efficient pulse width modulated source. A technical note with further details of the lens drive is available on our website [10].

All modelling data were made available to us by the manufacturer. Nevertheless, we checked the current vs. diopter relationship, at visible wavelengths, at a 25 degC temperature. The effective focal length of the lens was calculated by measuring object and image plane distances from the center element of the lens and applying the thin lens equation, appropriate to this lens thickness (3.1 mm maximum) used at relatively long object (1 m to 25 m) and image (>100 mm) distances. Measurements for three different lens samples were repeated. The results indicate that the lens' diopter values were proportional to lens current and followed the relationship:

$$diopter = (31 \pm 1) \times lens\ current(A) + (5.68 \pm 0.09)$$

2.2.2 Optical modeling and system design

The laparoscopic TLS was designed based on a number of considerations:

1- The system focus should be set by an electrically tunable lens, without external mechanics and capable of fast operation to enable autofocus system development.

2- Chromatic aberration and field curvature should be minimized in the visible and the NIR.

3- The imaging system should be constructed using off-the-shelf optical components.

4- Space to accommodate several fluorescence emission filters should be provided.

5- The system should be lightweight and compact.

The imaging system was modeled using ZEMAX optical ray tracing software, with lenses specifications obtained from their respective suppliers. The focus-tunable lens material has a refractive index of 1.3, an Abbe number of 105 and its contribution to chromatic aberration is thus low, but not negligible. Chromatic aberration compensation was achieved by selection of glasses in the other lenses and by optimizing the inter-lens distances. Modelling was performed at 450, 530, 600 and 800 nm. Chromatic focus shift modelling was performed up to 900 nm.

We designed the system for a nominal focal length of 28 mm. The focus tunable element then consumes <100 mA to minimize lens temperature rise; this is equivalent to a typical focus-tunable element focal length of ~130 mm, corresponding to a 40 mm radius of curvature. The range of system focal lengths covered is >26.5-29.5 mm, corresponding to 0-150 mA, and allows for both inter-laparoscope variations and short working distances operation. The system object was placed at infinity and an aperture of 2.8 mm diameter was selected to mimic the laparoscope exit pupil. We selected a configuration that places the focus-tunable

Biomedical Optics EXPRESS

element between two 12.5 mm diameter achromatic doublets, as shown in Fig. 2(a). Plano-concave lenses are used between the second achromatic lens and the sensor to reduce the field curvature; ideally aplanatic lenses, or thick meniscus lenses would have been used but these are not readily available off-the-shelf commercially. This configuration leaves plenty of room to place several excitation blocking filters between the eyepiece and the first achromat. Figure 2(a) shows the outline of the optical system and the details of the components for a 28 mm focal length configuration appropriate for a 1/3" sensor format. This provides an angular view of ± 34 degrees at the laparoscope entrance pupil, as calculated with the method described by Wang *et al.* [23]. The modulation transfer function (MTF) curves of the TLS for visible and NIR wavelengths approach the diffraction limit, as shown in Fig. 2(b). We also show in Fig. 2(c) the chromatic focus shift for our TLS. For comparison, we also show the chromatic focus shift for a commercial lens (#67-715, Edmund Optics) used in some of the *in vivo* experiments described in §2.3.1. Although both lenses performed well in the visible, our TLS halved the chromatic focus shift compared to the commercial lens over the visible-NIR region. However, the MTF curves for the commercial lens were almost identical to those of the TLS and were thus not plotted for clarity. Spot diagrams are provided in our technical note [10] and we show that all wavelengths in the 450-850 nm range are focused well within the Airy disc associated with 450 nm (12 μm diameter).

An alternative configuration where two image sensors are used to independently acquire color reflectance and fluorescence images is shown in Fig. 2(d). This permits the use of a NIR-optimized sensor and a high resolution color sensor. Such arrangements have been shown to have the advantage of independent processing of the NIR output for overlay purposes [9, 20, 24]. This alternative configuration uses the EL-10-30-TC lens closest to the eyepiece, followed by an achromatic lens pair and a dichromatic beam splitter. Space for additional filters is provided between the beam splitter and the sensors. Modelled optical performance comparable to the previous design (Fig. 2(a)) was achieved (results not shown).

Biomedical Optics EXPRESS

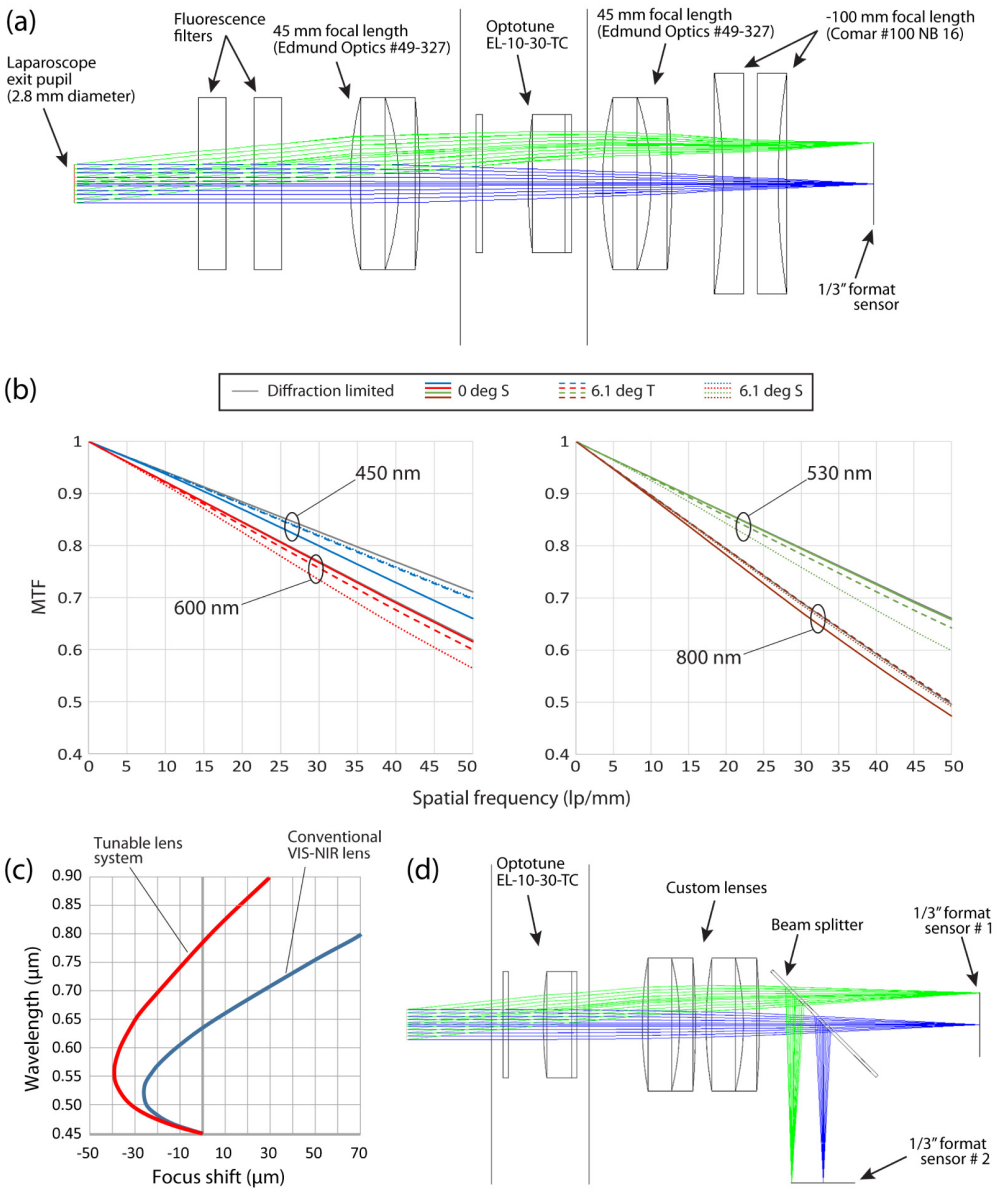

Fig. 2. (a) Optical ray tracing for a 28 mm focal length configuration (1/3" sensor format) of the TLS. The minimum (0 degrees) and maximum (6.1 degrees) field angles are shown in blue and green respectively. (b) Modulation transfer function (MTF) of the TLS for all system wavelengths and two field angles in the tangential (T) and sagittal (S) planes. The tangential 0 degree MTF curves are identical to the sagittal ones and were not plotted for clarity. MTF curves are displayed on two separate graphs for clarity. (c) The chromatic focus shift of the TLS is shown in red for comparison with the chromatic focus shift of a commercial VIS-NIR lens used for experiments described in section §3.2.2. (d) Ray trace modeling of an alternative TLS configuration that uses two separate sensors to image fluorescence and white reflectance. The custom achromatic lens pair comprises two 60 mm focal length lenses with different glass combinations (N-BK7/N-SF5 and N-BK7/N-SF10 respectively). The largest light ray angle at the beam splitter is ~ ± 3 degrees.

Biomedical Optics EXPRESS

2.2.3 Prototype development

The 28 mm focal length TLS described above was constructed in a custom housing. Figure 3(a) shows a CAD model of the assembly. All parts were machined from aluminum alloy 6082, matt black anodized. A 7 mm optical aperture was placed between the two plano-concave lenses to reduce potential diffuse and off-axis reflections. The final assembly is 48.5mm long (to camera CS-mount, excluding clamping mechanism), providing ~20 mm space for several filters which may be stacked in front of the TLS, its maximum diameter is 34 mm and it weighs 135 g. The TLS was designed to fit CS-mount cameras, although small adjustments can make it compatible with C-mount ones. An image of the TLS next to a conventional C-mount 28 mm coupler (LEOA28, Lenoptec, Shenzhen, China) is shown in Fig. 3(b).

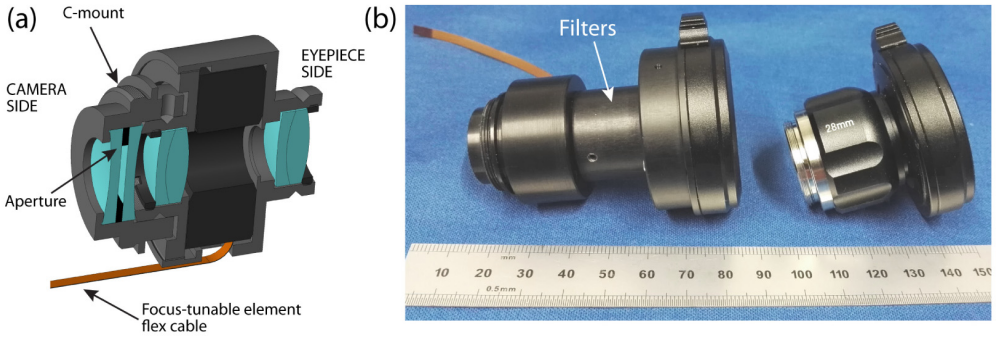

Fig. 3. (a) CAD section view of the custom housing that holds the optical components. (b) Image of the TLS (left) next to a conventional 28 mm laparoscope adapter (right). The generous space for filters could be readily reduced by 10 mm if required.

2.2.4 Optical characterization

A schematic representation of the experimental setup used to assess the optical performance of the lens system is shown in Fig. 4. The TLS was coupled to a 1.3 mega pixel (MP) CCD camera (BFLY-U3-13S2M-CS, Point Grey). The NIR blocking filter in front of the camera sensor was removed for optimal transmission in the range 450-900 nm. Image acquisition and camera control were performed using the Point Grey FlyCapture2 software.

The system was coupled to the eyepiece of the laparoscope using a custom-made clamp that allowed correct centration of the lens optical axis with the exit pupil. The laparoscope was mounted vertically and with the tip pointing downwards. A 1951 USAF resolution chart (R3L3S1N, Thorlabs) was placed in the object plane at a distance of 20 mm from the laparoscope tip. This short working distance was used to allow determination of the smallest feature that the laparoscope can resolve. Illumination was provided externally to avoid the typical uneven field illumination produced by the laparoscope optical illumination channel. This ensured a more accurate characterization of the lens optical performance. A halogen light source was used (LHS-H100C-1, Nikon) and its output light was collimated and passed through bandpass filters (450 ± 20 nm, 530 ± 26 nm, 600 ± 20 nm and 800 ± 20 nm, Thorlabs) mounted on a filter wheel (CFW6, Thorlabs). The center wavelengths corresponded to the ones used for modelling. The filtered output was focused on the input of a 5 mm diameter optical fiber bundle (Fostec-Schott), which produced an output beam with numerical aperture (NA) of 0.5. This beam trans-illuminated a 100 x 125 mm ‘opal’ diffusing glass screen (#02-149, Edmund Optics) onto which the resolution chart was placed.

Biomedical Optics EXPRESS

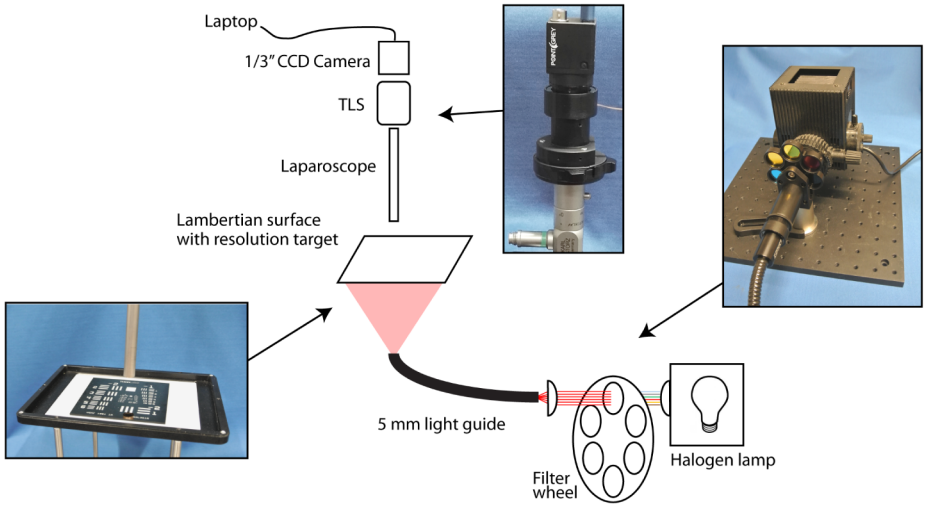

Fig. 4. Schematic and photographic (insets) representation of the experimental setup used to measure the optical performance of the lens system.

The performance at each wavelength band of the TLS, when used with the laparoscope was compared with that from the LEOA28 coupler, connected directly to the eyepiece. Optimal focus for both was set using either the 530 nm or 800 nm filters, depending on the experiment performed. Images were acquired at each illumination wavelength band by rotating the filter wheel. Camera exposure time was set to 40 ms and the intensity of the light source was adjusted for each filter in order to provide comparable detected signal intensity. All experiments were performed with minimal ambient light. Line profiles of representative regions of the images were extracted using ImageJ software (https://imagej.nih.gov/ij/). The Michelson contrast formula was used to calculate the contrast for each element of the USAF resolution chart:

$$\frac{I_{\max} - I_{\min}}{I_{\max} + I_{\min}}, \tag{1}$$

where $I_{\max}$ and $I_{\min}$ represent the highest and lowest pixel intensity values of adjacent bars within an element. Using the Rayleigh criterion, bars were considered resolved if the contrast value was greater than 0.26 [25]. The smallest chart element that could be resolved was determined for both the TLS and the LEOA28 coupler at each spectral channel.

The performance of the TLS, by itself, was determined using an experimental setup similar to that described above. The laparoscope was removed and a 2.8 mm aperture placed in front of the lens to replicate the model shown in Fig. 2(a). The lens-resolution chart distance was increased to 2 m to ensure that the lens focus is set to a value comparable to that used with the laparoscope. The MTF was computed by scaling the spatial frequencies of the resolution chart elements by the magnification of the optical system.

2.3 White light and fluorescence imaging

2.3.1 Experimental setup

The prototyped TLS was tested in an *in vivo* setup to assess the feasibility of fluorescence imaging. The lens was used in conjunction with 1/3" color CCD color cameras with NIR blocking filter removed; this does not alter the system color balance provided a 'cold' white light source (e.g. LED) is used. Narrow band notch filters (NF03-658E-25 and NF03-785E-25, Semrock, Rochester, USA) were placed in series between the TLS and the eyepiece to

Biomedical Optics EXPRESS

allow white reflectance imaging (following application of conventional white balance and gamma correction processes) and fluorescence imaging of two excitation channels. The excitation and illumination light was provided by an FGS imaging system previously described [21]. White light from an LED and red – NIR light from laser diodes (660 nm and 785 nm center wavelengths respectively) was delivered to the laparoscope illumination port using a 5 mm diameter liquid light guide (LLG20.530, Ultrafine Industrial Ltd., Rugby, UK). The camera was used with a maximum exposure time of 40 ms to ensure real time operation, as required for surgical navigation.

The TLS tuning range was tested by imaging a human hand with a laparoscope working distances varied over the range 10-100 mm. For this work, a very small drop of ICG from the tip a 27-gauge needle was applied to the back of the hand. The ICG was used at a nanomolar concentration, although this was difficult to quantify precisely due to the method of application. The 785 nm excitation wavelength was used with power density never exceeding 50 mW/cm^2.

For animal work, the laparoscope working distance was set to ~50 mm, resulting in excitation power densities of ~12 mW/cm^2 and ~25 mW/cm^2 for the 660 nm and 785 nm wavelengths respectively. Imaging performance was compared with our previous FGS imaging system which used a 25 mm focal length imaging lens (#67-715, Edmund Optics), with transmission optimized in the visible and NIR wavelengths.

2.3.2 Animal model

Animal procedures were carried out in accordance with the UK Animals (Scientific Procedures) Act 1986 and with local ethical committee approval. In the first experiment, OE33 human esophageal adenocarcinoma cells (5×10^6) diluted in RPMI serum-free medium were inoculated subcutaneously behind the front paw in three 42-49 day old female NOD SCID gamma (NSG) mice (Charles River, UK). These mice were kindly made available to us from a separate ongoing experiment. Mice were fed with an alfalfa-free diet to minimize autofluorescence. After 11 days all mice developed tumors. A fluorescently tagged peptide (EMI-137, EM Imaging, Edinburgh, UK) was used to target the OE33 tumor cells that are known to have high expression of human tyrosine kinase c-Met [26]. This probe has an excitation peak of ~650 nm, compatible with the 660 nm excitation channel of our system [27]. An aliquot of peptide solution (1.6 µg/20 g mouse) was injected intravenously into the tail vein. Mice were anesthetized using 2% isoflurane one hour after tracer injection. In the second experiment, a BALB-c nude mouse (Charles River, UK) was anesthetized and received 2 µg/20 g of ICG (Cardiogreen, I2633, Sigma Aldrich) freshly diluted in distilled water, by subcutaneous injection into the hind paw. Fluorescence excitation was delivered using the 785 nm channel and imaging was performed 2 min after tracer injection. All mice were kept under anesthesia throughout the imaging procedures.

3. Results

3.1 Optical characterization

The performance of the TLS by itself was assessed and compared with model predictions (Fig. 5(a)). Results at 530 nm and 800 nm show good agreement with theory. The lens was then tested in conjunction with the laparoscope using the experimental setup illustrated in Fig. 4. Images of the resolution chart at 450 nm, 530 nm, 600 nm and 800 nm are shown (Fig. 5(b)) for the TLS along with those using the LEOA28 coupler, both focused at 530 nm. Figure 5(c) shows line profile data taken across a region of interest corresponding to 4 line pairs/mm (lp/mm) at the object plane, demonstrating the superior performance of the TLS when used with the laparoscope. Line profiles of images acquired with just the TLS (i.e. no laparoscope) are also reported (black curves). Negligible variations of such line profiles

Biomedical Optics EXPRESS

across the range 450 – 800 nm suggest that the TLS itself is truly achromatic, as predicted by the theory.

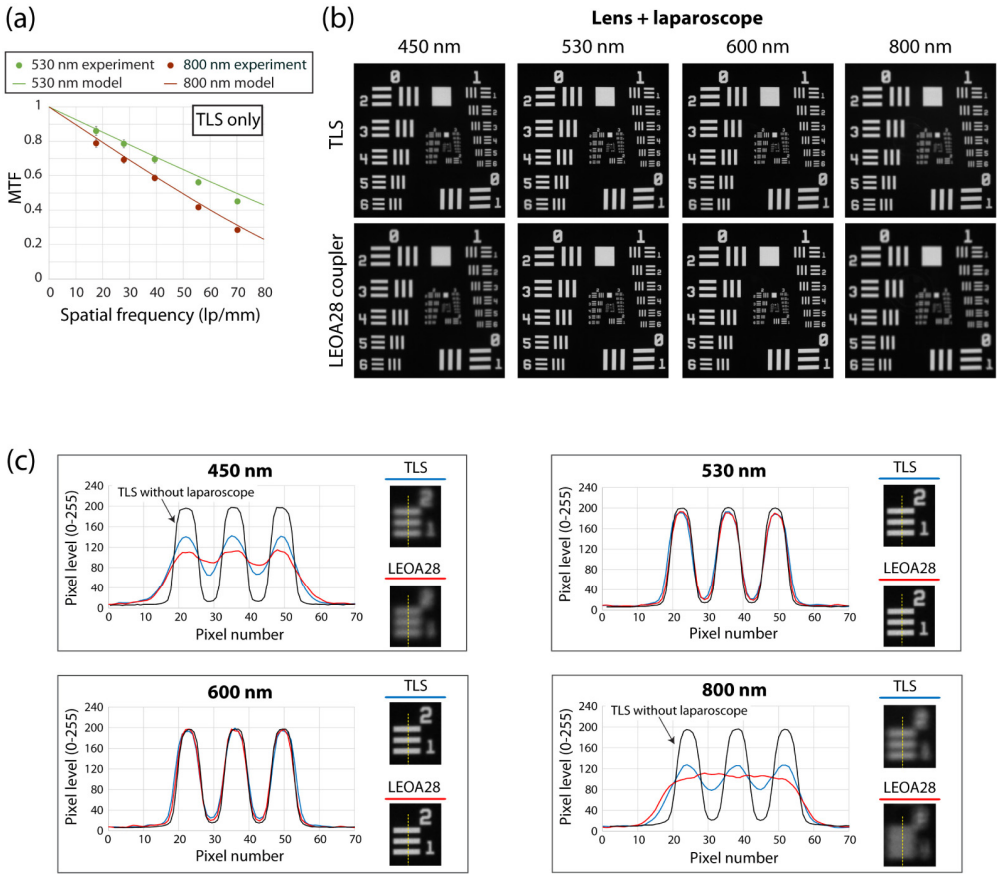

Fig. 5. (a) Experimental vs. modeled MTFs of the TLS at 530 nm and 800 nm illumination bands. Note that these results refer to the TLS used on its own (i.e. without laparoscope). (b) 1951 USAF resolution chart images for the TLS used with the laparoscope (top) and the LEOA28 coupler used with the laparoscope (bottom) at each spectral band and at a working distance of 20 mm. (c) Line profiles for a region of interest corresponding to group 2 element 1 (4 lp/mm) of the resolution chart. The black curves represent equivalent measurements obtained with the TLS used without laparoscope.

The theoretical (Airy disk) resolution, defined by the laparoscope output pupil diameter and by a notional 28 mm focal length lens used for imaging, along with the smallest resolvable elements when the TLS or the LEOA28 coupler were used with the laparoscope are shown in Table 1. Both systems had a resolution of 39 μm, when they were initially focused at 530 nm and performed close to the theoretical limit. It is noted that the USAF resolution target is inevitably quantized and this leads to uncertainty in defining the best resolution possible. Nevertheless, our TLS performs better at 450 nm, where the LEAO28 lens would be expected to work well, since it is designed for work in the visible. As modelling of the TLS indicates, an improvement is also observed at 800 nm, where we would not expect the LEAO28 to perform well. Imaging would be normally performed by focusing in the visible and these data show that the achievable resolution would indeed be limited by the laparoscope. Table 1 also shows the performance achievable when the laparoscope and associated imaging lens focus is set at 800 nm. As expected, performance degradation in the visible is noticeable, although the TLS is seen to perform better. Unfortunately, we were not

Biomedical Optics EXPRESS

able to obtain the optical prescription of the LEOA28 coupler from the manufacturer and so do not have access to its chromatic focus shift data.

Table 1. Resolution in object space at different illumination spectral bands.

Illumination wavelength	Theoretical resolution limit	TLS (focused at 530 nm)	LEOA28 coupler (focused at 530 nm)	TLS (focused at 800 nm)	LEOA28 coupler (focused at 800 nm)
450 nm	27.5 µm	112 µm	140 µm	62 µm	70 µm
530 nm	32.5 µm	39 µm	39 µm	177 µm	281 µm
600 nm	36.5 µm	39 µm	39 µm	157 µm	250 µm
800 nm	49 µm	125 µm	177 µm	50 µm	50 µm

TLS used in conjunction with the laparoscope at a working distance of 20 mm (tip to object plane), corresponding to a 5x demagnification between object and image planes.

3.2 White light and fluorescence imaging

An example of the need for short working distance in FGS and consequent need for refocusing is shown in Fig. 6. In Fig. 6(a) we present an image acquired with the TLS used with the laparoscope at a working distance approximate to that used during abdominal surgery; the small fluorescing region is hardly visible at this low magnification (ICG emission collected over a wavelength range of 802-840 nm). As the working distance is decreases, the fluorescing region becomes readily detectable. However, at the shorter working distances the detail available to the surgeon is very poor indeed (Figs. 6(c-d)), although refocusing reveals the required detail (Figs. 6(g-h)). Despite Fig. 6 not being obtained in a surgical environment, it nevertheless helps to show that both focusing and NIR achromatic performance are useful and are delivered by the TLS. The refocusing speed can only be appreciated from the supplementary movie (Visualization 1).

Figure 7 further demonstrates the feasibility of *in vivo* fluorescence imaging of the TLS when used with a laparoscope. A representative subcutaneous OE33 xenograft was visualized at 2 hours after injection of the EMI-137 peptide targeting c-Met (Figs. 7(a-c)). Detected fluorescence image wavelengths are in the range 673-700 nm. The images also show fluorescence emission from one of the kidneys, as a result of renal clearance of the tracer. Figures 7(d-f) shows fluorescence imaging of an inguinal lymph node (indicated with the yellow arrow) following subcutaneous injection of ICG in the left hind paw. The lymphatic vessels below the tissue surface were also clearly visible, confirming the desirable achromatic performance of the TLS coupled to the laparoscope.

A comparison of NIR fluorescence performance with our previous FGS imaging system is shown in Figs. 7(g-h); these images were acquired sequentially from the same animal, although some slight repositioning errors were inevitable. Lens focus was set such that the mouse skin was in focus when illuminated with white light. All images in Fig. 7 are snapshots of videos recorded at 25 fps. A typical example of such a video can be found in Visualization 2.

Biomedical Optics EXPRESS

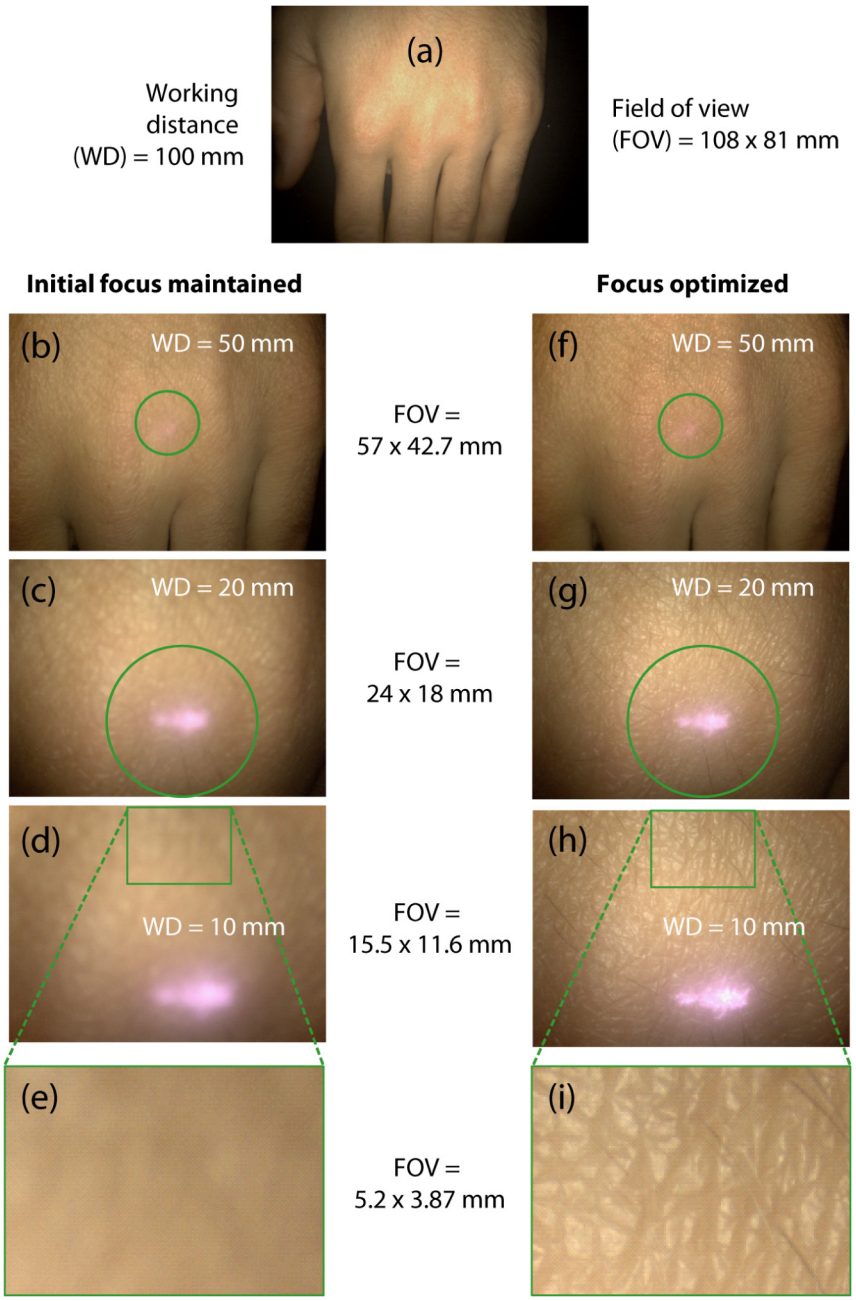

Fig. 6. Illustration for the need for focusing in high sensitivity FGS. (a) Initial scene, acquired at a working distance (WD) of 100 mm, typical of that used in abdominal surgery. Images (b-d) are acquired at progressively reduced WDs, without modifying initial focus set for image (a), nor excitation power density. Images (f-h) are acquired with focus optimized at each WD. Images (b, f) show why short WDs are useful: the fluorescing region is not readily identifiable and a WD reduction helps significantly in identifying the presence of a weak, low area fluorescing region (image (c)). Optimally focused images shown in images (g, h) show the need for focusing. Images (e) and (i) are magnified regions of images (d, h) respectively and further confirm the need for focusing to reveal detail adjacent to fluorescing region. WD is the object-to-laparoscope tip distance and not the object-to-objective distance, since the latter is placed within the laparoscope body.

Biomedical Optics EXPRESS

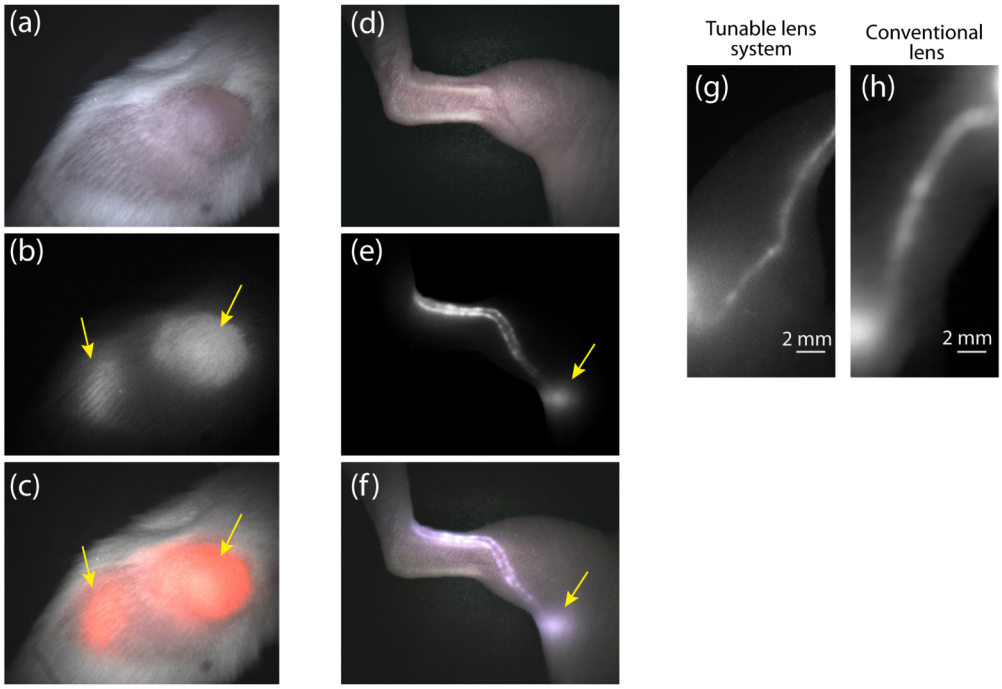

Fig. 7. *In vivo* evaluation of laparoscopic imaging. (a) White reflectance, (b) fluorescence and (c) combined fluorescence + white reflectance images of a subcutaneous tumor (right arrow), obtained with the TLS. Fluorescence signal of the probe accumulating in the kidney is also shown (left arrow). (d) White reflectance, (e) fluorescence and (f) combined fluorescence + white reflectance images of the left inguinal lymph node (arrows) following subcutaneous injection of ICG, obtained with the TLS. Lymphatic vessel fluorescence imaging of ICG using the TLS (g) in comparison with our previous imaging system that used an imaging lens optimized for use in the visible and NIR (h). Lens focus for both cases was set for white reflectance imaging.

4. Discussion

In this paper, we presented a novel achromatic, focus-tunable imaging lens system (TLS), compatible with most conventional laparoscopes, for application in fluorescence-guided surgery (FGS). Our system was designed to be readily replicated by other researchers involved in the development of novel clinical FGS approaches, as it can be constructed using off-the-shelf optical components. The TLS is based around an electrically focus-tunable fluidic lens which allows the use of control buttons rather than hand operated mechanical arrangements. Replacing the focus ring with appropriate buttons can considerably improve the ergonomics of the system, as the action of focusing and holding the laparoscope can be performed easily with the same hand. Moreover, this TLS opens the way to implementing an autofocus arrangement, where its fast response (<7.5 ms for a small signal step response [10]) is clearly useful. Even without an autofocus system, two or three preset focus points (Visualization 1) can go a long way towards achieving operation over a wide range of working distances since laparoscopes provide an acceptable depth of field at medium-long working distances due to their high f-number and short focal length. The use of external moving parts is avoided, enabling straightforward implementation in a research environment. The TLS allows convenient use of very short working distances (down to <10 mm), desirable for FGS and particularly fluorescence molecular imaging (FMI) in order to identify, rather than to operate on, sub-millimeter lesions with good sensitivity. Shorter working distances inevitably make instrument access awkward but are desirable, for example, to confirm surgical margins.

Biomedical Optics EXPRESS

Maximizing sensitivity is always desirable in FGS and FMI, but this is often hampered by the fact that a finite excitation power is available. Since all laparoscopes provide a wide excitation/detection field of view, excitation power density can be increased only when the working distance is decreased: this then causes a change in focus and our TLS can readily compensate for this.

We showed that our arrangement was achromatic in the visible and the NIR. In addition, when used in conjunction with a laparoscope intended for abdominal surgery and a 1/3" format CCD camera, it can achieve an achromatic performance superior to that from a conventional visible-NIR lens, with obvious advantages for simultaneous imaging of white reflectance and NIR fluorescence. However, the chromatic focal shift in the NIR due to non-optimized optical elements of the laparoscope is still noticeable and further work is required to correct for this. Since optical prescriptions from laparoscope manufacturers are generally difficult to obtain, our TLS can be used to derive the chromatic focus shift associated with laparoscopes by acquiring data from a set up similar to that shown in Fig. 4. Such data can be used to provide input to a ray tracing model. This approach will depend on inter-laparoscope variability and this remains to be determined. It is very likely that custom glass elements will be required to correct for these chromatic focus shifts and this may detract from an arrangement intended to be constructed without use of custom elements. Of course the rapid tunable feature of our system could be exploited to provide truly achromatic imaging in the NIR when used in conjunction with sequential white-NIR fluorescence imaging systems (e.g. such as described in [28]).

Our approach presents further advantages that contribute to improve the performance of an FGS laparoscopic system. Commercial laparoscope couplers usually use small diameter optics as they are placed very close to the eyepiece: it is then almost impossible to place custom fluorescence excitation blocking filters between the eyepiece and the coupler. Placing filters in this 'infinity' optical space is advantageous as angles of incidence are low in this space. Our focus-tunable element has a large clear aperture (10 mm) providing ample space for additional filters. The overall dimensions of our TLS are comparable with those of existing commercial couplers, facilitating clinical acceptance.

There have only been a few attempts of exploiting focus-tunable fluid lenses for minimally invasive surgery [29–31]. However, their aim was to develop zoom systems and they were not intended for fluorescence imaging neither in the visible nor the NIR. In addition, these models and prototypes were not compatible with standard laparoscopes. In contrast, our TLS can fit existing laparoscopes without major ergonomic differences and without interfering with standard laparoscopic procedures.

Most of the existing laparoscopic adapters/cameras provide a zoom control ring adjacent to the focus ring. Although this is used to accommodate different types of laparoscopes and endoscopes, intra-operative 'zoom' is typically provided by manually varying the tip-tissue distance [32]. It is noted that, in general, the use of image zooming during FGS results in wastage of available excitation power and is thus not encouraged. Despite the lack of a zoom feature, our TLS can be designed to have a given focal length to match a specific laparoscope/endoscope, although the clamp and associated mechanics are standardized. This is a reasonable compromise as similar procedures are typically performed with the same laparoscope-focal length combination. Our chosen focal length was 28 mm, which generated a viewing angle of ± 34 degrees using a standard 300 mm long, 10 mm diameter rigid laparoscope. This is a convenient value as it provides a field of view similar to conventional systems [23] and it excludes the outermost part of the ~ ± 38 degrees illumination beam, where the illumination intensity falls off significantly due to the typical Gaussian-like profile. This is even more crucial in fluorescence imaging, where the lower excitation power density near the edge of the beam results in poorer detection sensitivity.

We provided *in vivo* imaging results that showed the capability of the TLS to operate as part of an FGS setup. While performance checks using targets of phantoms are always useful,

Biomedical Optics EXPRESS

they do not readily replicate practical imaging requirements, where the imaged field is rarely flat, where fine tissue structures are present and where movement may degrade the modelled performance. Acquiring image data in preclinical experiments provided us with confidence for future clinical translation.

Funding

Cancer Research UK (C5255/A15935 and C1380/A18444); Oxford Cancer Imaging Centre (H3R00010).

Acknowledgments

The authors would like to thank David Leuenberger at Optotune for his help in obtaining a beta version of the EL-10-30-TC lens and for useful discussions. We also thank John Prentice and Gerald Shortland (Department of Oncology Mechanical Workshop) for manufacturing the lens housing, and Robert Newman (Electronics Workshop) for constructing the lens drive electronics. We are grateful to Dr Ian Wilson for supplying the EMI-137 c-Met targeting peptide.